

# Positive-Contrast Imaging in the Rabbit Hind-Limb of Transplanted Cells Bearing Endocytosed Superparamagnetic Beads

Warren D. Foltz,<sup>1</sup> Charles H. Cunningham,<sup>2</sup> Anthony J. Mutsaers,<sup>3</sup> Steven M. Conolly,<sup>4</sup>  
Duncan J. Stewart,<sup>1</sup> and Alexander J. Dick<sup>5</sup>

*Dept. of Cardiology, St. Michael's Hospital, Toronto, Ontario, Canada<sup>1</sup>*

*Dept. of Electrical Engineering, Stanford University, Stanford, California, USA<sup>2</sup>*

*Dept. of Medical Biophysics, University of Toronto, Toronto, Ontario, Canada<sup>3</sup>*

*Dept. of Bioengineering, UC Berkeley, Berkeley, California, USA<sup>4</sup>*

*Dept. of Cardiology, Sunnybrook and Women's College Hospital, Toronto, Ontario, Canada<sup>5</sup>*

## ABSTRACT

**Positive-contrast methods can augment negative-contrast methods for CMR evaluation of transplanted cell fate in vivo. This study correlated positive-contrast signal characteristics in the rabbit hind-limb with xenograft cell number (rat fibroblasts bearing endocytosed 1  $\mu\text{m}$  Bang's particles) at different stages of Gd-DTPA administration and 1mm<sup>2</sup> in-plane resolution (2 minute scans, 1.5 Tesla). Linear regressions modeled satisfactorily the cell number dependencies of signal-to-noise (SNR) and area-of-enhancement ( $R > 0.83$ ), over approximately a 50-fold fluctuation in cell number to a lowest detected limit of 25k cells during Gd-DTPA administration. Gd-DTPA administration elevated the slopes of parameter regressions by four or more standard deviations.**

## INTRODUCTION

Recently, there has been an increasing interest in the design of methodologies for non-invasive imaging of transplanted cells (1–5). These methodologies have the potential to enhance pre-clinical and clinical trials of cell therapy by providing novel end-point measurements of cell fate. Each of CMR, SPECT, and PET may prove to be particularly useful for cell-targeted imaging in large animal trials.

One rational strategy for cell targeted imaging is the intracellular loading of cells *ex vivo* with a superparamagnetic iron oxide contrast agent (6–8). In vivo these cells shift the resonance frequency of surrounding tissue water. Matching and mismatching of the remote and local tissue water resonance frequencies with a narrow bandwidth radiofrequency distribution appears

to be a principal image contrast mechanism in vivo with resultant positive or negative image contrast at the sites of labeled cells (9). In addition, there is an obvious enhancement of T2\* relaxation from the dipolar fields in the proximity of labeled cells. An observed T2 relaxivity enhancement is possibly consequent of diffusion local to small clusters of iron label (10).

The positive-contrast methodology of Cunningham et al. may facilitate quantification of CMR signal characteristics from the tissue water in the immediate proximity of transplanted cells (9). Potentially, one may then evaluate directly the number and physiological state of transplanted cells in vivo. Using a model of cell delivery into the rabbit quadriceps and hamstrings, this research demonstrates the correlations between cell number and simple signal characteristics on positive-contrast projection images (area of contrast enhancement and signal-to-noise ratio or SNR), at parameters consistent with large animal scanning in vivo (1-mm<sup>2</sup> in-plane resolution, 2 minute scans, 1.5 Tesla scanner). Benefits to cell transplant detectability of the T1 shortening effect on endogenous tissue water of gadolinium-diethyltriaminepentaacetic acid (Gd-DTPA) administration are demonstrated.

## METHODS

Studies were conducted in 12 3-5kg New Zealand white rabbits of both sexes with approval of the Internal Review Board of Sunnybrook and Women's College Health Sciences Centre.

Received 13 October 2005; accepted 11 April 2004.

Keywords: CMR, positive-contrast imaging, superparamagnetic beads, rabbit.

Correspondence to:

Warren Foltz, Ph.D.

8-038A Queen Wing, St. Michael's Hospital

30 Queen Street,

Toronto, Ontario

fax (416)480-5714

email: warren.foltz@sw.ca

The care and treatment of the animals was in accordance with relevant guidelines and statutes.

### Cell preparation

Rat fibroblasts between passages 3 and 6 were expanded at 38°C in fibroblast growth media (DMEM, Sigma-Aldrich, Oakville, Ontario, CA, 10% fetal bovine serum, and 2% penicillin/streptomycin; 8 ml per T75 flask). On the day prior to MR experimentation, 0.97  $\mu\text{m}$  diameter iron-fluorescent particles (IFPs, Bang's Laboratories, Fishers, Indiana, USA) were added to two confluent flasks (10  $\mu\text{L}$  IFP stock solution per ml of fibroblast growth media). Following an 18 to 24 hour incubation at 38°C for IFP endocytosis, the cells of each flask were rinsed twice with phosphate-buffered saline to remove naked IFPs, trypsinized (2.5 mL of trypsin), and centrifuged at 1000 rpm for 5 minutes. Cell suspensions in media at variable cell densities were created by serial 2:1 dilutions of cells, starting from an initial 500  $\mu\text{L}$  volume of media. The first dilution tended to contain 500000 (500 k) to 1200000 (1.2 M) cells, and the final dilution tended to contain from 20 to 60 k cells. Viable cell density at each dilution was calculated via Trypan Blue exclusion within 40 minutes of transplantation.

### Animal preparation

Each rabbit's hind-limb was prepared for cell delivery via surgical removal of the skin and underlying fascia under standard anaesthesia and analgesia (induction: 50 mg/kg ketamine and 5 mg/kg xylazine intra-muscular; maintenance: intravenous injection, as needed, of a 10 mL cocktail in saline, containing 20% ketamine and 10% xylazine). Remote target sites for cell injection were demarcated directly on the quadriceps and hamstrings using a black permanent marker, while each rabbit was positioned prone within the imaging head coil. A 140  $\mu\text{L}$  volume from each dilution of the cell suspension was extracted into a 250  $\mu\text{L}$  volume Hamilton precision syringe and injected into each target site through a 5/8" 27G needle. Rabbits were sacrificed following completion of imaging.

### MR imaging

All imaging was performed using a 1.5 Tesla GE Signa (General Electric Medical Systems, Waukesha, Wisconsin, USA). Imaging was completed between a 3 hour time window to minimize apoptosis and the redistribution of extracellular beads by macrophages. A total of 11 rabbits were scanned. Data in the absence of Gd-DTPA were acquired from 6 animals. Data following Gd-DTPA bolus infusion were acquired from 4 animals (0.15 mmol/kg). Data during Gd-DTPA steady-state infusion were acquired from 7 animals (~ 1 mL per minute of Gd-DTPA diluted in saline, 10 mmol Gd-DTPA in 270 mL saline, 40 minute equilibration time). Two animals were scanned under each experimental condition. Differences in the experimental protocols between animal groups were consequences of scan time limitations and a dynamically-changing protocol, representative of a shift from our preliminary efforts to correlate the Gd-DTPA partition co-efficient (measured using positive-contrast T1) with cell number.

The positive-contrast methodology enables selective T2-weighted imaging of the off-resonance water resonance frequencies, by employing a narrow RF bandwidth (1 kHz passband) tuned to roughly  $\pm 900$  Hz from the endogenous tissue water, combined with refocusing and a short readout (9). The pulse sequence is currently limited to spin-warp projection imaging. Projection images were obtained in a two minute time window at both positive and negative frequency offsets ( $\pm 900$  Hz center frequencies, TR = 500 ms, 2 averages, 256  $\times$  128, 20 cm FOV) within an oblique plane parallel to the hind-limb surface (Fig. 1a).

### Statistical analysis

Per region-of-interest (ROI) measurements were performed of both the area and SNR of positive-contrast enhancement, in non-blinded fashion and immediately after each individual experiment. ROIs for CMR data analysis at each injection site were drawn manually (xcinema, Stanford University, Palo Alto,

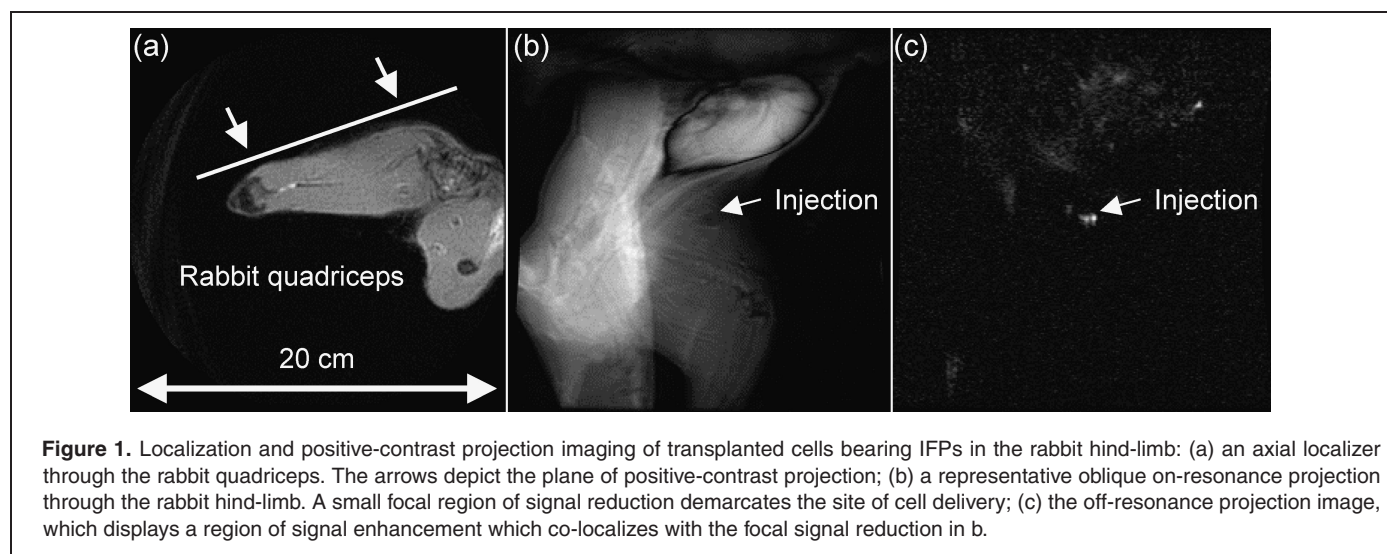


**Figure 1.** Localization and positive-contrast projection imaging of transplanted cells bearing IFPs in the rabbit hind-limb: (a) an axial localizer through the rabbit quadriceps. The arrows depict the plane of positive-contrast projection; (b) a representative oblique on-resonance projection through the rabbit hind-limb. A small focal region of signal reduction demarcates the site of cell delivery; (c) the off-resonance projection image, which displays a region of signal enhancement which co-localizes with the focal signal reduction in b.

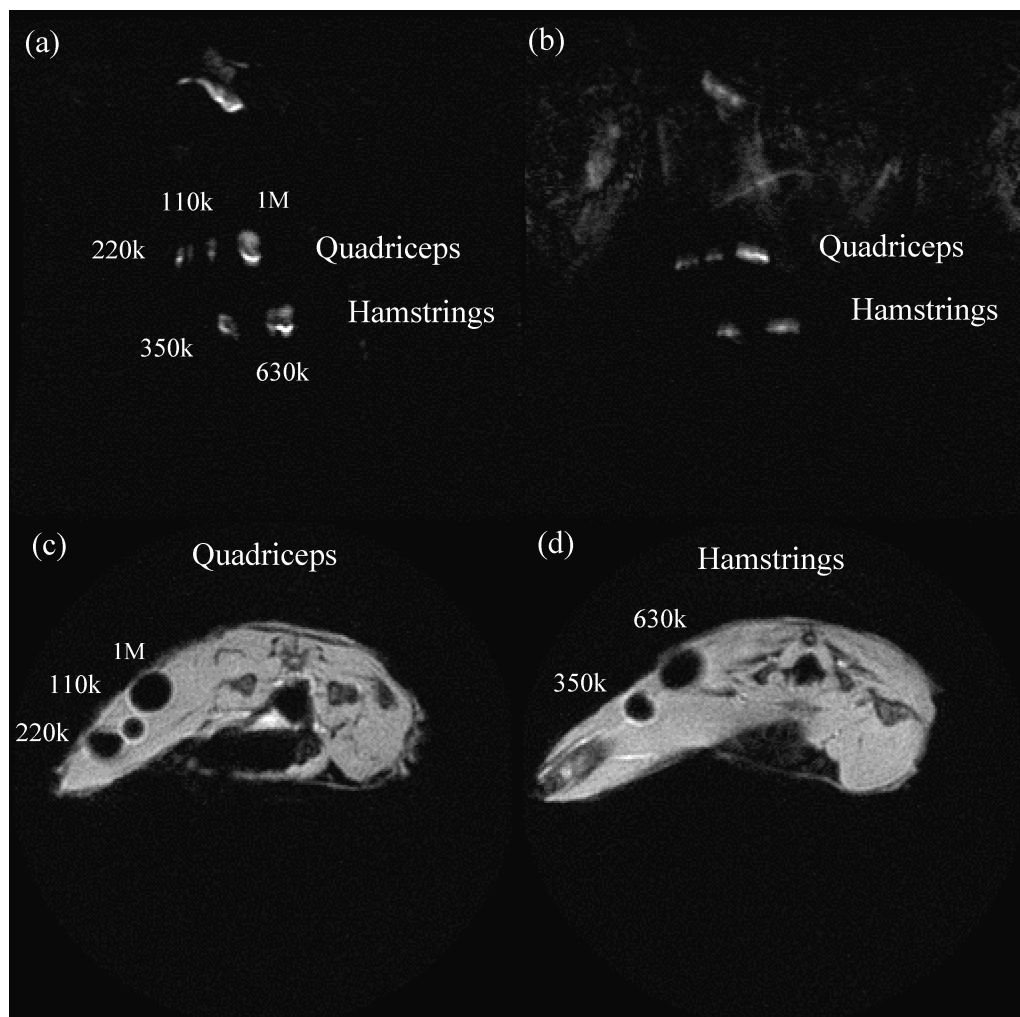


**Figure 2.** Representative images through a rabbit hind-limb bearing 5 injection sites of variable cell number from 110 k to 1 million cells. Projections of the cells' locations in the quadriceps and hamstrings, as per Fig. 1(a), are delineated as regions of positive-contrast at (a) +900 Hz and (b) -900 Hz. The approximate cell number injected at each site is demarcated in (a). Axial negative-contrast images prescribed through (c) quadriceps and (d) hamstrings sites of positive-contrast verify the locations of signal origin.

California, USA), including only pixels with a per voxel SNR greater than 6 for positive-contrast analysis to reduce operator dependence. Per voxel SNRs and areas were plotted with viable and transplanted cell number, as measured by Trypan Blue, for linear regression (OriginLab, Northampton, Massachusetts, USA).

## RESULTS

Fig. 1b and c depict the on-resonance and positive-contrast projections through an oblique plane oriented parallel to the hind-limb. A region of focal signal loss is evident in Fig. 1b at the location of signal enhancement in Fig. 1c. Fig. 2 demonstrates the cell number dependence of positive-contrast SNR and area-of-enhancement and verifies the origin of signals within the quadriceps and hind-limb. A site containing 100 k cells is

clearly delineated at both positive and negative frequency offsets at millimeter-scale resolution (Fig. 2a-b).

Regressions and regression analyses are summarized in Fig. 3 and Tables 1 and 2. Strong positive parameter regressions with transplanted cell number were consistently evident ( $R^2 \geq 0.68$ ). Gd-DTPA administration elevated the slopes of SNR and area regressions by up to 4 and 7 standard deviations respectively. Furthermore, Gd-DTPA increased both the consistency in detection of cell transplants of less than 250 k cells (Table 3) and the precision of cell number quantification from regression parameters. Precision of cell number quantification is characterized as a 'sensitivity' (Tables 1 and 2), defined as the relative increase in cell number which elevates the contrast area or SNR by a quantity equivalent to the 95% confidence interval of the slope under linear transformation ( $\Delta x/x > 2\sigma_B/B$ , expressed as a percentage, which is derivable by equating  $y = A+B(x+\Delta x)$

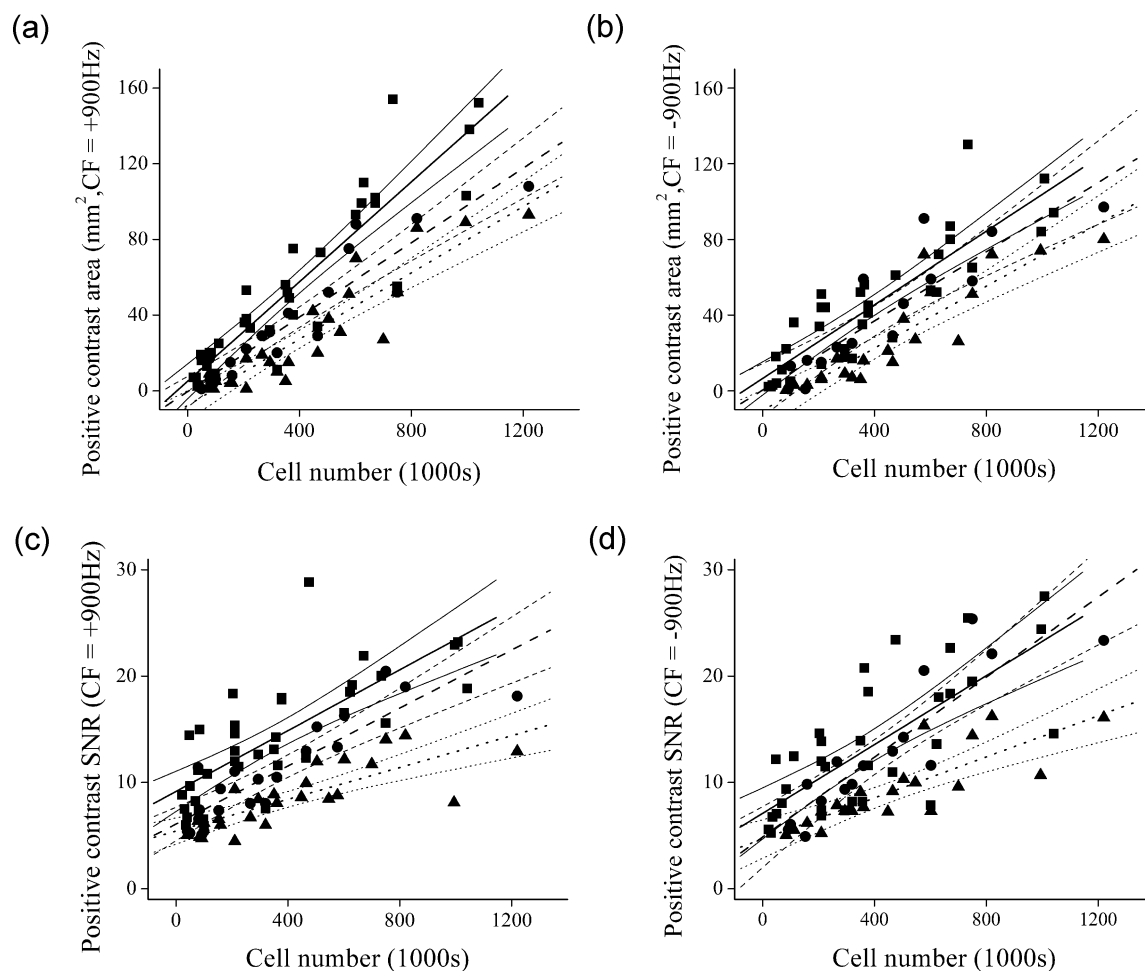


**Figure 3.** Linear regressions of positive-contrast enhancement area and SNR with transplanted cell number, including 95% confidence intervals, during three states of Gd-DTPA delivery (steady-state infusion: squares and solid lines; bolus injection: circles and dashed lines; no Gd-DTPA: triangles and dotted lines).

and  $y = A + (B + 2\sigma_B)x$ ). It varied from a low of 15% for area measurements during Gd-DTPA infusion to a high of 40% for SNR measurements in the absence of Gd-DTPA.

## DISCUSSION

Trials of cell therapy have demonstrated both safety and physiological benefits from vascular and intramuscular cell delivery

(12, 13). Continued improvements in trial results are expected as design modifications are implemented which increase the therapeutic and survival capacities of cells (14, 15). Imaging can guide the optimization of trials by providing non-invasive endpoints of transplanted cell fate.

An important observation obtained from pre-clinical cell delivery trials has been a correlation between therapeutic benefit and transplanted cell number (16, 17). The number of viable

**Table 1.** Linear regression of areas of enhancement and transplanted cell numbers ( $y = A + Bx$ ), for positive-contrast acquisitions at both offset resonance frequencies and under each state of Gd-DTPA delivery. The uncertainty is one standard deviation. All slopes (B) are elevated significantly from 0

	A(mm <sup>2</sup> )	B(mm <sup>2</sup> /1000 cells)	R <sup>2</sup>	Sensitivity(%)	#, data pairs	#, rabbits
+900 Hz, endog	-8 ± 4	0.09 ± 0.01	0.85	22	26	6
-900 Hz, endog	-10 ± 5	0.08 ± 0.01	0.81	25	21	6
+900 Hz, bolus	-1 ± 4	0.10 ± 0.01	0.88	20	21	4
-900 Hz, bolus	0 ± 7	0.09 ± 0.01	0.78	22	16	4
+900 Hz, ssGd	5 ± 5	0.13 ± 0.01	0.82	15	38	7
-900 Hz, ssGd	6 ± 4	0.10 ± 0.01	0.77	22	35	7

**Table 2.** Linear regression of per ROI SNR and transplanted cell numbers ( $y = A + Bx$ ), for positive-contrast acquisitions at both offset resonance frequencies and under each state of Gd-DTPA delivery. The uncertainty is one standard deviation. All regression parameters are elevated significantly from zero

	A(mm <sup>2</sup> )	B(mm <sup>2</sup> /1000 cells)	R <sup>2</sup>	Sensitivity(%)	#, data pairs	#, rabbits
+900 Hz, endog	5 ± 1	0.007 ± 0.001	0.68	29	26	6
-900 Hz, endog	5 ± 1	0.010 ± 0.002	0.81	40	21	6
+900 Hz, bolus	6 ± 1	0.014 ± 0.002	0.77	29	21	4
-900 Hz, bolus	5 ± 2	0.019 ± 0.002	0.78	21	16	4
+900 Hz, ssGd	9 ± 1	0.014 ± 0.002	0.83	29	38	7
-900 Hz, ssGd	7 ± 1	0.016 ± 0.002	0.86	25	35	7

transplanted cells may be increased by maximizing cell delivery (limited by needle pressure to about 10 million cells for each direct intramuscular injection but often 10 to 100-fold less [2]) and minimizing cell attrition (a 5 to 20-fold reduction even given autology (17, 18), encompassing sub-optimal retainment and apoptotic and necrotic cell death [17]). A four-order-of-magnitude variation in viable cell number may thus be expected in a serial cell-tracking study, which sets a lofty goal for the imaging scientist.

This research demonstrates experimentally the strong correlations between each of the SNR and area of the positive-contrast signal with transplanted cell number following intramuscular injection, over approximately a 50-fold fluctuation in cell number to a lowest detected limit of 25 k cells during Gd-DTPA administration. This SNR-limited detection threshold was achieved on a 1.5 Tesla imager using scan parameters which are particularly easy to implement (~2 minute scan time, ~1 mm<sup>2</sup> in-plane resolution). In comparison, the absence of Gd-DTPA seems to limit consistent detectability at millimeter-scales in large animal models to between 100 k and 200 k cells, a threshold observed in negative-contrast cardiac porcine studies (2). Future experiments may evaluate whether the methodology is adaptable for imaging sparse cell distributions within a large animal model, which may prove to be characteristic of the remnant engrafted cells subsequent to systemic or organ-specific arterial infusion (19). Intuitively, negative-contrast methods may be better suited for such tasks because the intravoxel volume fraction of water resonating at positive-contrast frequencies may be prohibitively small for imaging. Cell density will also impact T2\*. Quite possibly, the utility of the methodology is limited already by variability in cell density and intervoxel volume fraction, as evidenced

by the inconsistencies in detection of transplants bearing 25 k to 250 k cells (Table 3).

### Iron sensitivity

The sensitivity to intracellular iron of the positive-contrast strategy seems similar to that of the steady-state-free-precession (ssfp) methodology (20). Heyn's predicted SSFP detection limit of about 15 pg Fe at an SNR near 5 given 100 μm resolution maps to a detection limit of 15 ng Fe at an SNR near 5 given 1 mm<sup>2</sup> resolution in-plane. At the lowest tested limit of positive-contrast, 25 k cells bearing 1 μm diameter IFPs provided close to a per voxel SNR of 6 during Gd-DTPA infusion at 0.8 mm × 1.6 mm resolution in-plane. The total iron mass in these cells is about 125 ng, based on our own unpublished spectrophotometric measurements of iron mass in fibroblast cell suspensions (~5 pg Fe per cell). Based on our regression analyses, a projection through the associated injection site during Gd-DTPA infusion encompasses about 8 mm<sup>2</sup> or 8 image pixels. Thus a per mm<sup>2</sup> quantity of iron near 15 ng was detected at the lowest tested detection limit of positive-contrast. Note that our iron mass measurement is considerably lower than Shapiro's published result of 35 pg Fe per cell following endocytosis by hepatocytes of 0.97 μm particles (21) but consistent with Bowen's results using THP-1 cells and SPIOs (22). This discrepancy with Shapiro may result from the greater phagocytic capacity of hepatocytes (23).

### Quantitative cell tracking: feasibility

A non-invasive magnetic resonance probe of transplanted cell number should induce signal fluctuations which can be related to cell number using a standard curve or mathematical model.

**Table 3.** Benefits to cell transplant detectability of Gd-DTPA administration. The second column displays the fraction of transplants detected across all animals at each state of Gd-DTPA administration and the third column displays the cell numbers of undetected transplants

	Fraction detected	Cell numbers in undetected samples
+900 Hz, endog	26 of 31 (84%)	50 k, 60 k, 100, 110 k, 200 k
-900 Hz, endog	21 of 31 (68%)	40 k, 50 k, 60 k, 80 k, 80 k, 90 k, 100 k, 100 k, 150 k, 200 k
+900 Hz, bolus	21 of 22 (95%)	60 k
-900 Hz, bolus	16 of 22 (73%)	40 k, 50 k, 60 k, 80 k, 80, 85 k
+900 Hz, ssGd	38 of 38 (100%)	NA
-900 Hz, ssGd	35 of 38 (92%)	40 k, 80 k, 80 k

However, T2 relaxation displays a weak cell number dependence, which is counter to observations of predominant static dephasing (22) but possibly reflective of intracellular diffusion around small clusters of magnetic beads (24). T2\* relaxation displays a strong cell number dependence (11, 22), which may be non-linear because field non-uniformity reduces local to both loosely and tightly-clustered cells. Processes which elevate tissue levels of extracellular magnetic label (such as inadequate cell culture rinsing, xenograft apoptosis, or cellular discharge of label) may also bias relaxometry measurements. SNR fluctuations with cell number will be subject to confounding factors such as coil sensitivity and imaging parameters, while area fluctuations with cell number cannot account independently for spatial variations in cell density. Each of these parameters should also display a RF bandwidth dependence because frequency matching will select for different volumes of the dipolar or remote field surrounding cells bearing superparamagnetic iron (9). Possibly, an *in vitro* phantom could provide a standard curve for SNR and cell number calibration, consisting of cells of varying densities embedded until physiological conditions in low-gelling temperature agar (which remains fluid at 38°C) and including a priori knowledge of coil sensitivities and scaling of factors governing SNR.

### *Study limitations*

Inflammation, local to the injection site and probably exacerbated by non-autologous cell delivery, may elevate the Gd-DTPA distribution volume and subsequent T1 shortening. Repetition of the experimental protocol local to autologous cells and allowing for a sufficient delay for bruising to be alleviated would provide a useful comparison. The brevity of the experimental design, however, does impart an inherent insensitivity of the results to programmed cell death because the characteristic morphological changes occur over a time scale of 6 to 24 hours (25). The selection of fibroblasts was motivated in part by experimental simplicity, though these cells have proven therapeutic value as a vehicle for gene therapy (18). We expect that they will demonstrate a similar capacity for magnetic labeling to other non-professional phagocytes, including the bone marrow-derived mesenchymal cell which has shares morphological characteristics with the fibroblast.

### **CONCLUSIONS**

We have developed an *in vivo* model of cell delivery to the rabbit hind-limb to correlate positive-contrast signal characteristics with cell number, using scan parameters characteristic of large animal studies. Gd-DTPA-mediated elevations of signal area and SNR facilitated tremendously the detection of small transplants (<200 k cells), to a lower limit of 25 k cells. Linearities of parameter regressions support continued evaluation of feasibility of cell number quantification and cell fate characterization *in vivo*.

### **ACKNOWLEDGEMENTS**

The authors are indebted to Carrie Purcell and Judy Trogadis for their technical expertise, as well as to Dr. Gerald Proteau and Dr. Graham Wright for their knowledge and support.

### **REFERENCES**

1. Bulte J, Douglas T, Witwer B, Zhang S, Strable E, Lewis B, Zywickie H, Miller B, van Gelderen P, Moskowitz B, Duncan, I, Frank J. Magnetodendrimers allow endosomal magnetic labeling and *in vivo* tracking of stem cells. *Nat Biotech* 2001;19:1141–1147
2. Dick A, Guttman M, Raman V, Peters D, Pessanha B, Hill J, Smith S, Scott G, McVeigh E, Lederman R. Magnetic resonance fluoroscopy allows targeted delivery of mesenchymal cells to infarct borders in swine. *Circulation* 2003;108:2899–2904.
3. Wu J, Chen I, Sundaresan G, Min J, De A, Qiao J, Fishbein M, Gambhir S. Molecular imaging of cardiac cell transplantation in living animals using optical bioluminescence and positron emission tomography. *Circulation* 2003;108:1302–1305.
4. Wu J, Chen I, Wang Y, Tseng J, Chhabra A, Salek M, Min J, Fishbein M, Crystal R, Gambhir S. Molecular imaging of the kinetics of vascular endothelial growth factors gene expression in ischemic myocardium. *Circulation* 2004;110:685–691.
5. Kraitchman D, Tatsumi M, Gilson W, Ishimori T, Kedziorek D, Walczak P, Segars W, Chen H, Fritzges D, Izbudak I, Young R, Marcelino M, Pittenger M, Solaiyappan M, Boston R, Tsui B, Wahl R, Bulte J. Dynamic imaging of allogeneic mesenchymal stem cells trafficking to myocardial infarction. *Circulation* 2005;112:1451–1461.
6. Weissleder R, Cheng H, Bogdanova A, Bogdanov A. Magnetically labeled cells can be detected by MR imaging. *J Magn Reson Imag* 1997;7:258–263.
7. Arbab A, Bashaw L, Miller B, Jordan E, Lewis B, Kalish H, Frank J. Characterization of biophysical and metabolic properties of cells labeled with superparamagnetic iron oxide nanoparticles and transfection agent for cellular MR imaging. *Radiology* 2003;229:838–846.
8. Sykova E, Jendelova P. (Magnetic resonance tracking of implanted adult and embryonic stem cells in injured brain and spinal cord. *Ann NY Acad Sci* 2005;1049:146–160.
9. Cunningham C, Arai T, Yang P, McConnell M, Pauly J, Conolly S. Positive contrast CMR of cells labeled with magnetic nanoparticles. *Magn Reson Med* 2005;53:999–1005.
10. Bowen C, Zhang X, Saab G, Gareau P, Rutt B. Application of the static dephasing regime theory to superparamagnetic iron-oxide loaded cells. *Magn Reson Med* 2002;48:52–61.
11. Hill J, Dick A, Raman V, Thompson R, Pessanha B, Guttman M, Varney T, Martin B, Dunbar C, McVeigh E, Lederman, R. Serial cardiac magnetic resonance imaging of injected mesenchymal stem cells. *Circulation* 2003;108:1009–1014.
12. Strauer B, Brehm M, Zeus T, Kosterling M, Hernandez A, Sorg R, Kogler G, Wernet P. Repair of infarcted myocardium by autologous intracoronary mononuclear bone marrow cell transplantation in humans. *Circulation* 2002;106:1913–1918.
13. Assmus B, Schachinger V, Teupe C, Britten M, Lehmann R, Dobert N, Grunwald F, Aicher A, Urbich C, Martin H, Hoelzer D, Dimmerler S, Zeiher A. Transplantation of progenitor cells and regeneration enhancement in acute myocardial infarction (TOPCARE-AMI). *Circulation* 2002;106:3009–3017.
14. Zhang M, Methot D, Poppa V, Fujio Y, Walsh K, Murry C. Cardiomyocyte grafting for cardiac repair: Graft cell death and anti-death strategies. *J Mol Cell Cardiol* 2001;33:907–921.
15. Zhao Y, Courtman D, Deng Y, Kugathasan L, Zhang Q, Stewart D. Rescue of monocrotaline-induced pulmonary arterial hypertension

- using bone marrow-derived endothelial-like progenitor cells: efficacy of combined cell and eNOS gene therapy in established disease. *Circ Res* 2005;96:442–450.
16. Pouzet B, Vilquin J, Hagege A, Scorsin M, Messas E, Fiszman M, Schwartz K, Menasche P. Factors affecting functional outcome after autologous skeletal myoblast transplantation. *Ann Thorac Surg* 2001;71:844–851.
  17. Retuerto M, Schalch P, Patejunas G, Carbray J, Liu N, Esser K, Crystal R, Rosengart T. Angiogenic pretreatment improves the efficacy of cellular cardiomyoplasty performed with fetal cardiomyocyte implantation. *J Thorac Cardiovasc Surg* 2004;127:1041–1050.
  18. Campbell A, Kuliszewski M, Stewart D. Cell-based gene transfer to the pulmonary vasculature: Endothelial nitric oxide synthase overexpression inhibits monocrotaline pulmonary hypertension. *Am J Respir Cell Mol Biol* 1999;21:567–575.
  19. Baklanov D, Demuinch E, Thompson C, Pearlman J. Novel double contrast CMR technique for intramyocardial detection of percutaneously transplanted autologous cells. *Magn Reson Med* 2004;52:1438–1442.
  20. Heyn C, Bowen C, Rutt B, Foster P. Detection threshold of single SPIO-labeled cells with FIESTA. *Magn Reson Med* 2005;53:312–320.
  21. Shapiro E, Skrtic S, Koretsky A. Sizing it up: Cellular CMR using micron-sized iron oxide particles. *Magn Reson Med* 2005;53:329–338.
  22. Bowen C, Zhang X, Saab G, Gareau P, Rutt B. Application of the static dephasing regime to superparamagnetic iron-oxide loaded cells. *Magn Reson Med* 2002;48:52–61.
  23. Rabinovitch M. Professional and non-professional phagocytes: an introduction. *Trends Cell Biol* 1995;5:85–87.
  24. Muller R, Gillis P, Moiny F, Roch A. Transverse relaxivity of particulate CMR contrast media: from theories to experiments. *Magn Reson Med* 1991;22:178–182.
  25. Kolios M, Czarnota G, Lee M, Hunt J, Sherar M. Ultrasonic spectral parameter characterization of apoptosis. *Ultrasound Med Biol* 2002;28:589–597.